This is a preprint, the final version is subject to change, of the American Mineralogist (MSA)
Cite as Authors (Year) Title. American Mineralogist, in press.
DOI: https://doi.org/10.2138/am-2020-6841

REVISION 2 of ms #6841

Polymerization during melting of ortho- and meta-silicates: effects on Q species stability, heats of fusion, and redox state of MORBs.

H. Wayne Nesbitt[1,*], G. Michael Bancroft[2], Grant S. Henderson[3]

1 Dept. of Earth Sciences, Univ. of Western Ontario, London, Canada N6A 5B7

2 Dept. of Chemistry, Univ. of Western Ontario, London, Canada N6A 5B7

3 Dept. of Earth Science, University of Toronto, Toronto, Ontario M5S 3B1, Canada

*Corresponding author: hwn@uwo.ca

This is a preprint, the final version is subject to change, of the American Mineralogist (MSA)
Cite as Authors (Year) Title. American Mineralogist, in press.
DOI: https://doi.org/10.2138/am-2020-6841

ABSTRACT

^{29}Si NMR and Raman spectroscopic studies demonstrate that fusion of crystalline orthosilicates and metasilicates produces melts more polymerized than their precursor crystals. Forsterite, for example, consists of 100% Q^0 species whereas its melt consists of ~50 mol% of Q^1 species (Q = a Si tetrahedron and the superscript indicates the number of bridging oxygen atoms in the tetrahedron). Polymerization during melting can be rationalized from an energetics perspective. Si-NBO-M moieties of Q species are more susceptible to librational, rotational and vibrational modes than are Si-BO-Si moieties (NBO = non-bridging oxygen; BO = bridging oxygen; M = counter cation). Thermal agitation activates these additional modes, thus increasing the C_p and free energy of melts. Reaction of Q^n to Q^{n+1} species during melting eliminates Si-NBO-M moieties and produces Si-O-Si moieties which are less susceptible to the additional modes, thereby minimizing the C_p of melts. By decreasing the abundances of Q^0, Q^1 and Q^2 species in favor of Q^3 and Q^4 species, melts become more stable. In the absence of polymerization, melting temperatures of minerals would be appreciably greater than observed.

Polymerization involves formation of Si-O bonds, which is strongly endothermic (Si-O bond dissociation is ~798 kJmol^{-1}). The large heats of fusion (ΔH_f) of orthosilicates result primarily from polymerization reactions during melting (ΔH_f of forsterite, fayalite and tephroite are ~142, ~92 and ~90 kJmol^{-1}). Fusion of metasilicates and sorosilicates (e.g., pyroxenes and melilites) involves endothermic polymerization *and* exothermic depolymerization reactions, although the former dominates. These reactions tend to negate each other during melting, yielding less positive ΔH_f values than observed for orthosilicate fusion (e.g, ΔH_f of enstatite, diopside, pseudowollastonite and åkermanite are ~73, ~69, ~57 and ~62 kJmol^{-1}). Where

polymerization and depolymerization reactions are absent, ΔH_f is low and is due to mostly to disordering during melting (e.g., ΔH_f of cristobalite is ~8.9 $kJmol^{-1}$).

Experimental evidence indicates that ferric iron is present as a *negatively charged* oxy-anionic complex in melts (e.g, $[FeO_2]^{1-}$) so that oxidation of Fe^{2+} should proceed according to:

$$4Fe^{2+}_{melt} + 1O_2 + 6O^{2-}_{melt} \rightarrow 4[FeO_2]^{1-}_{melt}$$

Free oxygen (O^{2-}), a by-product of polymerization reactions, drives the reaction to the right. MORBs consequently should be more oxidized than their source (e.g., lherzolites) or their residues (e.g., harzburgites). Extraction of melt from the upper mantle and deposition in the crust should produce a crust more oxidized than its upper mantle source. Production of O^{2-} during melting and its presence in alkali-rich magmas also explains the *alkali-ferric iron effect*.

Keywords: silicate melting, Mantle melting, Q species energetics, heats of fusion, polymerization reactions, MORB redox reactions

INTRODUCTION

The upper mantle consists mostly of olivines and pyroxenes, with minor feldspar, spinel or garnet, and their melting gives rise to basaltic and komatiitic magmas (Frost, 2008, and references therein). To understand better the production of the magmas, experimental evidence related to melting of orthosilicates, sorosilicates and metasilicates is summarized in an attempt to identify the reactions and reaction mechanisms by which these phases melt. The melting mechanism of metasilicates has been previously elucidated (Nesbitt et al., 2017a,b) but the reactions and mechanisms by which other mantle minerals melt have not. Some reactions

involved in the melting of a number of minerals are here identified and their energetics are explored. One such reaction is the polymerization reaction where two tetrahedra (Q species), each incorporating at least one NBO, react to produce BO and free oxygen (Nesbitt et al., 2017c; 2015; 2011). Although the extent to which polymerization reactions proceed in melts may be small, they nevertheless decrease NBO concentrations in the melt and increase BO and free oxygen (O^{2-}). Finally, free oxygen, a product of polymerization may affect redox reactions in melts and this aspect is addressed to obtain a better understanding of the redox chemistry of basaltic and komatiitic magmas and of the redox state of crust and upper mantle.

The degree of polymerization of silicate glasses and melts commonly is evaluated from their bulk compositions using NBO/T where T = moles of Si and NBO represents the moles of non-bridging oxygen in a glass (Mysen and Richet, 2019, p. 118). NBO/T is readily calculated for alkali silicate *crystals* in that the moles of alkali equals the moles of NBO, so that crystalline SiO_2, $Na_2Si_2O_5$, Na_2SiO_3, $Na_6Si_2O_7$ and Na_4SiO_4 have, for example, NBO/T ratios of 0.0, 1.0, 2.0, 3.0 and 4.0 respectively. The same holds for binary alkaline earth silicate crystals except that each mole of an alkaline earth = 2 moles of NBO so that NBO/T = 2.0 for enstatite ($MgSiO_3$) and 4.0 for forsterite (Mg_2SiO_4). The stoichiometric relationship between the moles of alkalis or alkaline earths and NBO *does not hold* for melts and glasses, primarily because polymerization reactions proceed in melts which produces a third oxygen species, free oxygen or O^{2-}. Some counter cations will bond to O^{2-} rather than to NBO, thus the stoichiometric relationship between NBO and counter cations does not hold. The consequence is that NBO/T cannot be accurately calculated from bulk melt or glass compositions and instead it must be determined from experimental Q species abundances (see Table 1, footnote 1 for calculation) or

by direct measurement of NBO (e.g., Nesbitt et al., 2011).. This aspect has not been previously addressed in the literature and is now emphasized using examples.

Six ^{29}Si MAS NMR or Raman spectroscopic studies of Mg_2SiO_4 and $CaMgSiO_4$ are listed in Table 1 (last column) and their NBO/T values average 3.46 rather than 4.0, as expected for the orthosilicate composition and as found for orthosilicate crystals (see Table 1, footnote 1, for calculation of NBO/T from experimental data). Similarly, NBO/T for five experiments on $MgSiO_3$, $CaSiO_3$ and $Ca_{0.5}Mg_{0.5}SiO_3$ glasses average 1.86 (Table 1) rather than the expected 2.0 for the metasilicate composition. The results of Table 1 make it obvious that NBO/T values of *glasses* cannot be evaluated from bulk glass compositions but must be determined experimentally, either by measurement of Q species abundances as in Table 1, or by direct measurement of NBO (e.g., Nesbitt et al., 2015; 2011). The reason for the low NBO/T values in the glasses relates to polymerization reactions occurring during melting (Nesbitt et al., 2015). These reactions consume some NBO and produce BO and free oxygen (i.e., $2NBO^- \rightarrow BO+O^{2-}$), yielding NBO/T values less than predicted from bulk glass composition. These NBO/T values of Table 1 are the evidence that polymerization reactions occur during melting. Finally, the free oxygen content of glasses can be calculated from NBO/T values as outlined in Table 1 (footnote 2) and O^{2-} values are listed in Table 1 (2^{nd} last column). The realization that NBO/T of melts and glasses cannot be predicted, and that polymerization reactions occur during melting of crystals, has spurred our investigation into the extent to which polymerization reactions proceed during melting of forsterite, fayalite, monticellite (orthosilicates), åkermanite (sorosilicate), enstatite, diopside and pseudowollastonite (metasilicates).

Crystalline orthosilicates consist of Q^0 species whereas the pyroxenes and pyroxenoids

consist of Q^2 species and the reactions related to melting must be different for each. There are four *independent* polymerization reactions, $Q^0 \rightarrow Q^1$, $Q^1 \rightarrow Q^2$, $Q^2 \rightarrow Q^3$ and $Q^3 \rightarrow Q^4$ (Nesbitt et al., 2017a; 2017b; Stebbins, 1987; Masson et al., 1970; Toop and Samis, 1962a, 1962b) and we focus on these. This is, to our knowledge, the first attempt to identify these reactions and discuss their implications for partial melting of the upper mantle. No new spectroscopic or calorimetric results are presented but a large number of existing results are utilized to identify the types of reactions that occur prior to and during melting (e.g., Nesbitt et al., 2015; Sawyer et al., 2015, 2012; Nasikas et al., 2012; 2011; Davis et al., 2011; Nesbitt et al., 2011; Kalampounias et al., 2009; Sen et al., 2009; Sen and Tangeman, 2008; Richet et al., 1998; 1996; 1994; 1993). With reactions identified, attention is directed to reaction mechanisms.

A by-product of polymerization reactions is free oxygen, O^{2-}, or oxide ion. Magnien et al., (2008), Borisov et al. (2017) and Cicconi et al. (2015) demonstrate that at liquidus temperatures O^{2-} and O_2(gas) affect or control Fe redox reaction rates and oxidation states in melts approaching basaltic compositions (~50 mole% SiO_2). Free oxygen production during partial melting of the upper mantle consequently may alter the redox state of mid-oceanic ridge basalts (MORBs) and other basalts generated in the upper mantle (Kress and Carmichael, 1989; 1988; Carmichael and Nicholls, 1967; Fudali, 1965). The effect of O^{2-} on the redox states of basaltic-komatiitic melts and on the crust and upper mantle are discussed.

SUMMARY OF EXPERIMENTAL STUDIES

Introduction

Melts contain a suite of Q species whereas the crystal from which the melt is derived typically incorporates only one Q species (e.g., Stebbins, 1987; Brawer and White, 1975). The

new Q species produced in the melt are necessarily produced through polymerization and disproportionation reactions. The nature, direction and extent of these reactions can be evaluated provided the Q species abundances in a melt and its precursor crystal have been determined (e.g., Sawyer et al., 2015; 2012; Nesbitt et al., 2015; 2011; Retsinas et al., 2014; Nasikas et al., 2012; 2011; Davis et al., 2011; Kalampounias et al., 2009; Sen et al., 2009; Sen and Tangeman, 2008; Dalby et al., 2007; George et al., 1998; Richet et al., 1998; 1996; 1993; Zhang et al., 1997; Frantz and Mysen, 1995; Mysen and Frantz, 1994; 1993; 1992; Maekawa et al., 1991).

On the assumption that the abundances reported by these studies represent the equilibrium distribution of Q species in a melt (at the glass transition temperature, Richet, 2001), one can determine which Q species are produced or consumed by comparing the Q species abundances in melt and precursor crystal. With this information, one may then deduce the types of reaction that have occurred during and immediately after melting. This approach is applied to melting of orthosilicates (e.g., olivines), metasilicates (e.g., pyroxenes) and other crystals.

Spectroscopic results for orthosilicates

Mg_2SiO_4. ^{29}Si MAS NMR experimental data for Mg_2SiO_4 glass is illustrated in Figure 1a. Sen and Tangeman (2008) interpret the narrow peak at -62 ppm to represent forsterite, which contains only Q^0 species. The broad peak centered at -71 ppm represents Q^0 and Q^1 contributions of the glass and based on their ^{17}O NMR spectrum, they report Q^0:Q^1 to be ~49:51. They suggest that the shoulder at ~ 80 ppm is a Q^2 glass signal which is reasonable considering its chemical shift. We have added a peak to fit the shoulder and it represents ~10% of the total glass spectral intensity. There is, then ~44% Q^0, ~46% Q^1 and ~10% Q^2 in the glass; hence ~56% of Q^0 species of the original crystal have undergone polymerization during melting (Table 1). ^{29}Si

NMR results of Davis et al. (2011) for Mg_2SiO_4 yield similar Q species abundances (Table 1).

The Raman spectrum of Mg_2SiO_4 glass is illustrated in Figure 1b and following Bancroft et al. (2018), a 50% Lorentzian-50% Gaussian lineshape was fit to the low frequency side of the band. It is interpreted as a Q^0 band (Voronko et al., 2006) and represents ~50% of the total signal. The shaded area of Figure 1b represents all other contributions and based on Raman shifts, the shaded area consists of mostly Q^1 and Q^2 species (McMillan, 1984). They constitute about half the spectral intensity which is consistent with the NMR results (Table 1). The Raman study of Kalampounias et al. (2009) also yields a similar Q species distribution in Mg_2SiO_4 glass consistent with the other results (Table 1). The presence of Q^1 and Q^2 species in Mg_2SiO_4 glass indicates polymerization of Q^0 occurs during melting of forsterite.

Fe_2SiO_4. The Raman spectrum of Fe_2SiO_4 glass displays a strong, broad signal between ~800-1100 cm^{-1} (Cooney and Sharma, 1990, their Fig. 2). It includes a comparatively low frequency band centered at ~850 cm^{-1} which is the frequency expected of a Q^0 signal (McMillan, 1984) and is interpreted as the Q^0 peak of Fe_2SiO_4 glass. There is also a very strong shoulder in the 900-1100 cm^{-1} region, which is of greater intensity than the shoulder on the Mg_2SiO_4 glass spectrum (Fig. 1b). Cooney and Sharma (1990) attribute the shoulder to abundant Q^1 and Q^2 species in the glass, a result of polymerization reactions during melting. The above-noted studies are consistent in demonstrating that fusion of the two major components of olivine produce melts appreciably more polymerized than their precursor crystals.

$CaMgSiO_4$. The ^{29}Si and ^{17}O NMR experimental results of Nasikas et al. (2012) report ~61% Q^0 and ~39% Q^1 species in $CaMgSiO_4$ glass (Table 1). In a separate Raman study, Nasikas et al. (2011) obtained 50% Q^0, 35% Q^1, 13% Q^2 and 2% Q^3 species in $CaMgSiO_4$ glass

(Table 1). Piriou and McMillan (1983, their Figs. 3 and 4) report Raman spectra of monticellite and $CaMgSiO_4$ glass. The spectrum of the latter includes a strong band at ~854 cm^{-1}, which is interpreted as a Q^0 signal (McMillan, 1984). There is also an intense high frequency shoulder that extends to about 1100 cm^{-1} and based on Raman shifts, the shoulder likely represents Q^1 and Q^2 species (McMillan, 1984). The NMR and Raman results for $CaMgSiO_4$ demonstrate that this orthosilicate melt (and glass) is more polymerized than its crystalline precursor.

Spectroscopy of the Sorosilicates

Raman spectrum of åkermanite ($Mg_2CaSi_2O_7$) indicates only a Q^1 species, but upon melting and quenching, the Raman spectrum of the glass reveals the presence of Q^0, Q^1 and Q^2 species (Sharma et al., 1988). The melting of this sorosilicate thus demonstrates that both polymerization and depolymerization reactions have occurred. Although little more can be said without quantification of the glass spectrum, the occurrence of both types of reaction are also observed in metasilicate glasses.

Spectroscopy of the Metasilicates

The metasilicate crystals consist of Q^2 species arranged in chains or rings, and they include the pyroxenes, pyroxenoids, pseudowollastonite, Na_2SiO_3 and Li_2SiO_3. Nesbitt et al. (2017a) elucidated the reactions and mechanisms by which Na_2SiO_3 melts and it is an excellent analogue for the melting of all Q^2 crystals.

$MgSiO_3$. Sen et al. (2009) report ^{29}Si MAS NMR results for $MgSiO_3$ glass for which Q^1:Q^2:Q^3:Q^4 ~ 25:42:26:7 (Table 1). The proportions indicate that ~25% of the Q^2 species of the crystal were *depolymerized* but that ~33% (25.7+7.3) were *polymerized* during melting. Their results are confirmed by the ^{29}Si 2D MAF NMR study of Davis et al. (2011) which are

summarized in Table 1. To summarize, ~58% of Q^2 species of enstatite undergo polymerization or depolymerization reactions during melting.

$CaSiO_3$ and $Ca_{0.5}Mg_{0.5}SiO_3$. The 2D ^{29}Si NMR study of Zhang et al. (1997) on $CaSiO_3$ glass yields ~55% Q^2 species, ~20% Q^1+Q^0 species and ~25% of Q^3+Q^4 species (Table 1). Polymerization reactions dominate in that $Q^3+Q^4 > Q^1+Q^0$ in the glass. Whether wollastonite or pseudowollastonite is melted, ~45% of the Q^2 species of the precursor crystal undergo polymerization or depolymerization reactions with the former dominating.

The Raman studies of $Ca_{0.5}Mg_{0.5}SiO_3$ by Retsinas et al. (2014) and Schneider et al. (2000) indicate that ~40% of Q^2 species of diopside undergo polymerization or depolymerization reactions, with the former reaction dominating (Table 1). The melting characteristics of the four Q^2 minerals enstatite, diopside, pseudowollastonite and wollastonite are qualitatively similar, with polymerization dominating depolymerization during melting.

Na_2SiO_3 and Li_2SiO_3. Richet et al. (1996) collected the Raman spectra of crystalline Na_2SiO_3 and Li_2SiO_3 melt (Fig. 2). The strongest band in both spectra is located at ~950 cm^{-1} and is interpreted as a Q^2 band (Richet et al., 1996). The crystal spectrum of Na_2SiO_3 (Fig. 2a) includes a weak Q^1 band and a Q^3 band (Nesbitt et al. 2017a). The Raman spectrum of the melt (Fig. 2b) indicates an appreciable increase in Q^3 species intensity upon melting but the intensity in the Q^1 region does not increase appreciably. The same relations are observed in the Raman spectra of crystalline Li_2SiO_3 and its melt (Richet et al., 1996; 1994). Comparison of Figures 2a and 2b reveal that polymerization reactions (production of Q^3 from Q^2) dominate depolymerization reactions (production of Q^1 species from Q^2) during melting. The same conclusion applies to the Li_2SiO_3 system.

This is a preprint, the final version is subject to change, of the American Mineralogist (MSA)
Cite as Authors (Year) Title. American Mineralogist, in press.
DOI: https://doi.org/10.2138/am-2020-6841

REACTIONS LEADING TO MELTING

Reactions preceding melting

Prior to melting, cation disordering occurs in many crystals. NBO-Na and NBO-K bond dissociation commences at ~700-800 K in Na_2SiO_3 and K_2SiO_3, NBO-Ca bond dissociation at ~1500-1600 K in diopside and pseudowollastonite. NBO-Mg bond dissociation occurs at ~1700 K in proto-enstatite, at ~2060 K in forsterite and at ~1390 K in fayalite (Nesbitt et al., 2017a,b; Bouhfid et al., 2002; Thiéblot et al., 1999; George et al., 1998; Dimanov and Jaoul, 1998; Dimanov and Ingrin, 1995; Richet et al., 1994; 1993; Orr, 1953). Mysen and Richet (2019, Chap. 3, p. 212) and Nesbitt et al. (2017a) argue that bond dissociation proceeds according to:

$$\text{Si-NBO-M} \rightarrow \text{Si-NBO}^- + \text{M}^+ \quad (1a)$$

$$2\text{Si-NBO-M} \rightarrow 2(\text{Si-NBO}^-) + \text{M}^{2+} \quad (1b)$$

and that thermal agitation is responsible for NBO-M bond dissociation. Apparently, above a threshold temperature, a fraction of total NBO exists as NBO^- (e.g., Cormack et al., 2002) and a fraction of the cationic sites are vacated with the cation delocalized. Equilibrium thermodynamic considerations require the fraction of both NBO^- and cation to be constant at constant temperature so that the mass action equation of Eq. 1 is obeyed. The fraction of both NBO^- and delocalized cations will be very small at low temperatures but the fraction should increase with temperature due to increased thermal agitation (Nesbitt et al., 2017b; Cormack et al., 2002). Nesbitt et al. (2017b, Fig. 5) estimate the fraction of delocalized Na^+ in crystalline Na_2SiO_3 and it increases from effectively 0% at 600 K to ~2.5% at ~1350 K_3. There should be an equivalent change in NBO^-. The fraction of both delocalized Na^+ and NBO^- will be still greater at greater temperatures where melts are stable.

Si-NBO$^-$ is negatively charged and it is a strong nucleophile (Lewis base) capable of attacking Si centers of Q species (Hamlin, 2018; Bento and Bickelhaupt, 2007;Laidler, 1965). Its production is the first step leading to melting of orthosilicates and metasilicates (e.g., Nesbitt et al., 2017a).

Orthosilicate melting Reactions

Cation disorder ensues at ~2060 K in forsterite (Richet et al., 1994), producing some Mg^{2+} and Si-NBO$^-$ in the crystal (i.e., $[Mg_{3/2}\text{-}Q^0]^{1-}$ in Fig. 3a). Through thermal agitation, Si-NBO$^-$ may approach and react with a Si center of an adjacent Q^0 tetrahedron ($[Mg_2\text{-}Q^0]^0$) to produce the dimer $[Mg_{3/2}\text{-}Q^1]^0$ according to (Fig. 3a):

$$[Mg_{3/2}\text{-}Q^0]^{1-} + [Mg_2\text{-}Q^0] \rightarrow 2[Mg_{3/2}\text{-}Q^1]^0 + 1/2Mg^{2+} + O^{2-} \quad (2a)$$

Ignoring the counter cation and dividing by two:

$$Q^0 \rightarrow Q^1 + 1/2O^{2-} \quad (2b)$$

The reaction likely proceeds as a nucleophilic substitution (S_N) reaction via an activated complex in which Si is five-fold coordinated (e.g., Mysen and Richet, 2019; Hamlin et al., 2018; Nesbitt et al., 2017a; Bento and Bickelhaupt, 2007; Laidler, 1965). The Q^2 species observed in Fig. 1a may also form via a S_N reaction where the nucleophile $[Mg_{3/2}\text{-}Q^0]^{1-}$ attacks a Q^1 species of Si_2O_7 to form a trimer (Si_3O_{10}) according to (Fig. 3b):

$$[Mg_{3/2}\text{-}Q^0]^{1-} + [Mg_2\text{-}Q^0]^0 \rightarrow 2[Mg_{1.5}\text{-}Q^2]^0 + 1/2Mg^{2+} + O^{2-} \quad (3a)$$

Ignoring the counter cation and dividing by two:

$$Q^1 \rightarrow Q^2 + 1/2O^{2-} \quad (3b)$$

Melts derived from fayalite and monticellite also include Q^1 and Q^2 species (Cooney and Sharma, 1990; Nasikas et al., 2011) and these crystals likely follow melting reactions analogous

to that of forsterite (Rxns. 1b, 2 and 3). NBO-M bond dissociation is a necessary first step in melting of orthosilicate crystals and at (or immediately above) the melting temperature, Reactions 2 and 3 proceed to produce Q^1 and Q^2 species in orthosilicate melts, thus explaining these Q species in the orthosilicate glasses.

Metasilicate melting reactions

Na_2SiO_3 melting proceeds in three steps (Mysen and Richet, 2019; Nesbitt et al., 2017a). As they describe, the first step is production of Si-NBO^- through NBO-M bond dissociation (Rxn. 1) where the nucleophilic moiety, Si-NBO^-, remains attached to its Q^2 chain. With increased thermal agitation, Si-NBO^- approaches and reacts with a Q^2 species on an adjacent chain to produce a Q^3 species $([M_1\text{-}Q^3]^0)^-$ which form cross-chain linkages. With M^+ as modifier cation, the reaction is:

$$[M_1\text{-}Q^2]^- + [M_2\text{-}Q^2]^0 \rightarrow 2[M_1\text{-}Q^3]^0 + M^+ + O^{2-}. \quad (4a)$$

or simplified:

$$Q^2 \rightarrow Q^3 + 1/2O^{2-} \quad (4b)$$

$[M_1\text{-}Q^2]^-$ is the reactant nucleophile. The Q^3 species form random cross-chain linkages along the Q^2 chains (e.g., Nesbitt et al., 2017a,b) thereby stabilizing the chains against thermal agitation. As evidence, at high temperature the Q^3 species band is observed in the Raman spectrum of Na_2SiO_3 (Fig. 2a) and similar high frequency bands are observed in the Raman spectra of $CaSiO_3$ and Li_2SiO_3 (Richet et al., 1998; 1996). Formation of Q^3 species, however, does not fragment the Q^2 chains as required for melting (Nesbitt et al., 2017a). Instead, fragmentation of the Q^2 chains occurs through attack by the very strong nucleophile O^{2-} generated by Reaction 4 (Mysen and Richet, 2019; Nesbitt et al., 2017a) according to:

283 $$2[M_2\text{-}Q^2] + Mg^{2+} + O^{2-} \rightarrow 2[M_3\text{-}Q^1] \quad (5a)$$

284 $$Q^2 + 1/2O^{2-} \rightarrow Q^1 \quad (5b)$$

285 where Q^1 forms as terminal species on Q^2 fragments (Fig. 4a). The reaction proceeds via a S_N
286 reaction mechanism (Fig. 4a). Under equilibrium melting conditions, Reactions 4 and 5 proceed
287 at constant rates thereby maintaining a constant O^{2-} concentration while the crystal melts (Mysen
288 and Richet, 2019; Nesbitt et al., 2017a). We propose that all metasilicates melt by the same
289 mechanism (i.e, Rxns. 1, 4, 5).

290 **Q^1 species Abundance.** Figure 2 indicates that Q^1 constitutes ~10 mol% of Q species of
291 crystalline Na_2SiO_3 just below its melting temperature. Although Reaction 5 causes melting
292 through fragmentation of Q^2 chains with Q^1 terminating the fragments, the Q^1 species abundance
293 has not accumulate appreciably in Na_2SiO_3 melt. Instead, Q^3 increases appreciably (compare
294 Figs. 2a and 2b) indicating that that a polymerization reaction consumes Q^1 and produces Q^3
295 species during melting. Apparently, after formation of Q^1 species during chain fragmentation,
296 the Q^1 species reacts with a Q^2 species of an adjacent chain fragment to produce Q^3 species (Fig.
297 4b) according to:

298 $$Na_3\text{-}Q^1 + Na_2\text{-}Q^2 \rightarrow Na_2\text{-}Q^2 + Na_1\text{-}Q^3 + 2Na^+ + O^{2-} \quad (6a)$$

299 and simplifying:

300 $$Q^1 \rightarrow Q^3 + O^{2-} \quad (6b)$$

301 The sum of Reactions 5 and 6 yields the *overall melting Reaction* 7 which is:

302 $$2(Na_2\text{-}Q^2)^0 \rightarrow 2(Na_1\text{-}Q^3)^0 + 2Na^+ + O^{2-} \quad (7a)$$

303 $$Q^2 \rightarrow Q^3 + 1/2O^{2-} \quad (7b)$$

304 The melting reaction thus involves Reactions 1, 4, 5, and 6, with Reaction 7 representing the

overall or stoichiometric melting reaction. The evidence is found in the crystal and melt spectra of Li_2SiO_3, $CaSiO_3$ and $CaMgSi_2O_6$, collected just below and above their melting temperatures. They indicate that Q^3 species abundances increase relative to Q^2 and Q^1 species in the melts relative to the crystals (e.g., Fig. 2 and Richet et al., 1998; 1996). Reactions 4 to 6 and the overall Reaction 7 probably occur during melting of all metasilicate crystals.

Polymerization of the melt via Reaction 7 should continue with heating until the rate of a depolymerization reaction offsets its effect, and the amount of O^{2-} produced should also increase with temperature until there are commensurate rates of depolymerization and polymerization.

REATION MECHANISM AND ENERGETICS

Summary of reaction mechanism

Polymerization and depolymerization reactions proceed in silicate systems via nucleophilic substitution (S_N) reactions where Lewis bases attack Si centers of tetrahedra to form Si^V-bearing activated complexes of near trigonal bipyramidal shape (Figs. 3 and 4; Mysen and Richet, 2019; Hamlin et al., 2018; Nesbitt et al., 2017a; Bento and Bickelhaupt, 2007; House, 1997; Laidler, 1965; Budd, 1961). The three major Lewis bases of silicate systems are BO, NBO and free oxygen (O^{2-}) which are referred to as nucleophiles in the kinetics literature (House, 1997; Laidler, 1965; Budd, 1961). BO is a weak nucleophile because its charge is moderated by bonds to two associated Si atoms and it is effectively immobile (Demiralp et al., et al., 1999). NBO-M bond dissociation produces the nucleophilic species $Si\text{-}NBO^-$ which, with loss of the cation, is somewhat mobile due to thermal agitation. It is a strong nucleophile (e.g., Nesbitt et al., 2017a; Hsieh et al., 1994, their Table 4) and it *initiates* polymerization and depolymerization reactions in silicate systems (Mysen and Richet, 2019; Nesbitt et al., 2017a). As polymerization

reactions proceed, a much stronger nucleophile, O^{2-}, is produced and its accumulation in crystals ultimately causes melting (Mysen and Richet, 2019; Nesbitt et al., 2017a).

Q species energetics and melt stability

The spectroscopic results of Table 1 demonstrate that the orthosilicate and metasilicate melts are more polymerized than their precursor crystals. An implication is that Q^0 is less stable than the more polymerized Q^1 and Q^2 species in orthosilicate melts and that Q^2 is less stable than Q^3 species in metasilicate melts. Polymerization reactions result in the replacement of O-M bonds (M = counter cations) by stronger O-Si bonds (Speight, 2005). Apparently, enthalpic gains associated with O-Si bond formation more than offset entropic losses associated with polymerization within the melt, at least for conditions near the melting temperatures. The explanation for enthalpic dominance may relate to normal modes available to Q^0, Q^1 and Q^2 species in melts relative to those available to Q^3 and Q^4 species.

Q^0 and Q^1 species. NBO-M bond dissociation and loss of a cation from its 'cationic site', destabilizes all NBO and BO atoms constituting the anionic polyhedral 'cage' surrounding the vacated cationic site (e.g., Nesbitt et al., 2017a; Richet et al., 1994; Cormack et al., 2002). These NBO and BO atoms tend to repel each other thereby setting up new librational, vibrational or rotational modes all of which contribute to the C_p of the melt. The Q^0, Q^1 and Q^2 species, with their high proportion of NBOs, are particularly susceptible to acquisition of new modes whereas Q^3 and Q^4 species are less so, because they remain bonded to three or four other tetrahedra via BO-Si bonds thus inhibiting acquisition of new modes.

An extreme in rotational and librational modes associated with a Q^1 species is illustrated in Figure 5a where the NBOs have lost their counter cation partner and have become 'unpinned'

from their structural sites. As drawn, the Q^1 species displays one rotational degree of freedom, which contributes ½R per mole of Q^1 to C_p (Davis, 1965; R is the gas constant). The Q^1 species also undergoes libration in two dimensions (one within and one out of the plane of the paper). Libration includes both kinetic and potential energy terms so that each librational mode contributes 1R per degree of freedom; thus *rotational and librational* modes of the Q^1 species (Fig. 5a) contribute 2½R per mole of Q^1 to C_p of the melt, which with the Debye contribution (~3R at high T), almost doubles the Q^1 C_p contribution to the melt (Davis, 1965; Moelwyn-Hughes, 1961). The coordination number of Mg in Mg_2SiO_4 melt is ~6 (Kohara et al., 2011) so that each dissociated NBO-Na bond produces up to ~6 tetrahedra with 'unpinned' NBO atoms, all being susceptible to acquisition of new modes. C_p of a melt may be increased substantially as a result. The arguments apply to all Q species containing NBO but they are particularly pertinent to Q^0 or Q^1 species.

Polymerization reactions should inhibit or quench some rotational and librational modes associated with the Q^0 and Q^1 species, thereby stabilizing the melt by decreasing its C_p and internal energy. The arguments are supported by an XPS valence band study of Na-silicate glasses (Nesbitt et al., 2017d). The results demonstrate that BO-Si binding energies are located in the lower valence band and Si-NBO bands in the upper valence band, separated by 2-6 eV. Conversion of NBO to BO stabilizes glasses, making them less energetic and less reactive.

Q^2 species. The shaded region of Figure 5b emphasizes the C_p increase within the premelting region of Na_2SiO_3 (Richet et al., 1998; 1996; 1994; 1993; Richet and Fiquet, 1991). The Debye vibrational, Na and O contributions account for C_p of the crystal up to the premelting region (Nesbitt et al., 2017b; Richet, 2001) but they cannot explain the dramatic C_p increase

within the premelting region. We propose that where NBO-M bonds of Q^2 species are ruptured, the tetrahedra containing 'unpinned' NBO atoms become susceptible to libration about the axis of the BO-BO chain, with librational from positions #1and #2 of Figure 6a, giving rise to *limited librations* within a deep potential energy well shown in Figure 6b. Increased thermal agitation results in more energetic excited states being populated, and with sufficient heat, the potential energy well may be topped (Fig. 6b), resulting in '*pronounced libration*' of the Q^2 tetrahedron (Fig. 6a, oscillations between positions #1 and #3). This type of configurational contribution would increase C_p within the premelting region.

Pronounced libration of a Q^2 tetrahedron must impose a torque on adjacent tetrahedra of Q^2 chains or rings, causing them to librate. The libration may be transmitted along the chain, giving rise to new, low frequency librational modes. In crystals with long Q^2 chains, libration may occur along the entire chain, dramatically increasing C_p. This may partially explain the exceptional increase in C_p within the premelting regions of Q^2 crystals (e.g., Fig. 5b). These low frequency librations are inhibited or quenched with fragmentation of the chains or rings, such as occurs during melting, thus explaining the abrupt *decrease* in C_p of the system once melting has occurred.

Consumption of Q^0, Q^1 and Q^2 species to produce more polymerized species via Reactions 2, 3 and 7, tends to stabilize melts by inhibiting or quenching new vibrational, librational and rotational modes. Without the polymerization reactions, melts would be less stable (greater free energies) and the melting temperatures of orthosilicate and metasilicate crystals would be greater than observed. Similarly, fragmentation of Q^2 chains during melting inhibits or quenches low frequency vibrations and librations from being transmitted along the

chains or around rings thereby stabilizing melts relative to crystals.

IMPLICATIONS

Magnitudes of the Heats of Fusion

The heats of fusion (ΔH_f) of silicates range from very large to small values. H_f of forsterite is ~142 kJmol^{-1} whereas that of cristobalite is 8.9 kJmol^{-1} (Richet et al., 1993; Richet and Bottinga, 1986). Melting of cristobalite involves no polymerization or depolymerization and ΔH_f results primarily from disordering during melting. The extent of disordering may be estimated using order-disorder theory where H_f is given by (Moelwyn-Hughes, 1961, p. 745):

$$\Delta H_f = (3/N_0)R(1-s_m^2)T_m \quad (8)$$

N_0 = the sum of the moles of species A (here the Q^4 species) and the number (or moles) of voids (holes) that A may occupy in the crystal structure. N_0 is taken as 2.0 in the subsequent calculation (i.e., there is one hole per Q^4 species in SiO_2 crystals). R is the gas constant, s_m the degree of order in the melt and T_m is the melting temperature (K) which is 1999 K (Richet and Bottinga, 1986). Where the crystal and melt is perfectly ordered, $s_m = 1.0$ at T_m. The degree of disorder of SiO_2 melt (s_m) is unknown but a value of $s_m = 0.8$, substituted into Equation 8, yields the measured ΔH_f value of 8.9 kJmol^{-1}. Apparently, SiO_2 melt retains a high degree of order upon melting. If the melt were completely disordered ($s_m = 0.0$), ΔH_f would equal 25 kJmol^{-1}. This cursory exploration of disorder indicates that its contribution to ΔH_f is rather small.

The Si-O bond dissociation energy is ~798 kJmol^{-1} whereas M-O bond dissociation energies are about half to one quarter this value (Speight, 2005) so that Si-O bond formation or dissociation energies are likely to be the dominant contribution to heats of fusion where polymerization reactions occur (e.g., Rxn 2). The heat of fusion of the orthosilicates, forsterite,

fayalite and tephroite are respectively ~142, ~92 and ~90 kJmol^{-1} (Richet et al., 1993; Richet and Bottinga, 1986). With respect to the metasilicates, Q^1 and Q^3 are produced during melting of these Q^2 crystals (Table 1) so that *both* polymerization and depolymerization reactions proceed during melting as previously discussed (Rxns 6 and 5 respectively). The reactions should tend to cancel one another resulting in the heats of fusion being less than for orthosilicate melting. Enstatite and diopside ΔH_f values are ~73 and ~69 kJmol^{-1} (per mole of Si, Richet and Bottinga, 1986) and pseudowollastonite is ~57.3 kJ/mol (Swamy and Dubrovinsky, 1997; Richet et al., 1994). Crystalline Na_2SiO_3 and Li_2SiO_3 have ΔH_f values of 52.2 and 12.2 kJmol^{-1} respectively (Richet et al., 1994; Richet and Bottinga, 1986). All are lower than ΔH_f of the orthosilicates. The heats of fusion of the Q^2 crystals are nevertheless endothermic, indicating that polymerization dominate depolymerization during melting. Finally, the Raman spectrum of $Mg_2CaSi_2O_7$ glass indicates that both depolymerization (to produce Q^0) and polymerization (to produce Q^2) proceed upon melting of åkermanite (Sharma et al., 1988). Its heat of fusion is ~62 kJmol-1 (normalized to 1 mol of Si), indicating that polymerization dominates depolymerization during melting. The magnitudes of the heats of fusion of the orthosilicates, metasilicates and åkermanite are consistent with the hypothesis that polymerization reactions dominate the energetics of melting of these silicates.

Incongruent melting of $MgSiO_3$

Bowen and Anderson (1914) demonstrated that crystalline $MgSiO_3$ (clino-enstatite) melted incongruently to forsterite and a melt where the melt was slightly more siliceous than $MgSiO_3$. Their explanation for the peritectic relationship was that clino-enstatite was unstable at its melting point (1830 K). This is, however, a restatement of the observation, rather than an

explanation. The peritectic relationship can be rationalized from the perspective of polymerization reactions by noting that crystals with large H_f have melting curves (liquidi) of shallow slopes near their congruent melting points (Krauskopf and Bird, 1995) whereas those with small H_f have steeper slopes. The enthalpies of fusion of forsterite, enstatite, diopside and cristobalite are respectively, in kJ/mole (of Si), 142±20, 73±6, 69±1 and 9±1 (Thiéblot et al., 1999; Richet et al., 1993; Richet and Bottinga, 1986; Richet et al., 1982; Kracek et al., 1937). The large heat of fusion of forsterite results in a shallow liquidus that extends beyond the $MgSiO_3$ composition, resulting in the peritectic melting of clino-enstatite. The peritectic melting relationship results primarily from the large enthalpy of fusion of forsterite which results from the extensive polymerization of the melt during fusion.

Upper mantle melting and Redox Reactions

^{29}Si NMR results of synthetic melts approaching basaltic-to-komatiitic compositions consist of ~11-12% Q^4 species, ~48-58% Q^3 species and ~30-41% Q^2 species (Morizet et al., 2015) and from these Q species abundances, the NBO/T values are calculated to be ~1.2-1.3. Morizet et al. (2015) obtained similar NBO/T values (0.93 to 1.1), based on their 'basaltic' glass compositions (T = mostly Si and Al). The NBO/T of fertile upper mantle source rocks (e.g., lherzolites) is decidedly greater than 1.3 in that NBO/T = 4 for olivines and ~2 for pyroxenes, the two phases contributing most to the melts. If the NBO/T of the basaltic/komatiitic glasses of Morizet et al. (2015) are representative, then natural basaltic and komatiitic melts are more polymerized than their mantle source rocks. Free oxygen (O^{2-}) is a necessary by-product of all silicate polymerization reactions so that it must also be present in basaltic and komatiitic melts produced in the upper mantle, and it must be available for reaction with other species.

Magnein et al. (2008) emphasize that at and above liquidus temperatures, oxygen diffusion via O^{2-} and gaseous O_2 determines the rate of Fe oxidation/reduction in silicate melts containing ~50 mol% SiO_2 (which approximate basalts and komatiites). Holmquist (1966) reviewed and summarized the evidence for Fe speciation in $Na_2Si_2O_3$ melt and concluded that ferric iron was present as a negatively charged oxy-anionic species of general formula $[FeO_x]^{(3-2x)}$ where $x > 1$. The simplest of these is $[FeO_2]^{1-}$ and it is employed subsequently. Using the data of Johnston (1965), Holmquist (1966) proposed the following reaction between ferrous and ferric species in the melt:

$$4Fe^{2+} + O_2 + 6O^{2-} \rightarrow 4[FeO_2]^{1-} \quad (9)$$

where O_2 is oxygen gas. Introduction of O^{2-} on the left side of the reaction is required to balance the charges on the Fe species and the stoichiometric coefficients are determined *solely by the effective charges* on the iron species involved. They *are not* determined by the coordination numbers of the species. Goldman (1983) subsequently demonstrated the validity of Reaction 9 using stoichiometric and thermodynamic arguments. As apparent from the stoichiometric coefficients, O^{2-} is 6 times more influential than O_2 in affecting the redox state of Fe in melts. The chemical species portrayed in Reaction 9 do not reflect coordination numbers, as indicated by the following analogy. The chemical species $[Fe(OH)_4]^-$ is present in aqueous solutions but this complex does not reflect its coordination number, which is 6. Similarly, the complex $[FeO_2]^-$ of the melt does not reflect the coordination number of Fe^{3+} in melts. Additional study is required to clarify the stoichiometry of the ferrous and ferric species in melts.

Redox state of basalts

Frost and McCammon, (2008) emphasize that Fe^{3+}/Fe^{2+} does not vary appreciably in

MORBs, whether they are the product of limited (e.g., ~6%) or substantial (~20%) partial melting of the upper mantle. Frost and McCammon, (2008) argue further that the constancy of the ratio cannot be explained by crystal-melt partitioning where Fe^{3+} is considered an incompatible element. Finally, they note that the constancy of the ratio cannot be explained by Reaction 10 because the O_2 concentration is too low to buffer ferric-ferrous ratios in melts.

$$2FeO + 1/2O_2 \rightarrow Fe_2O_3 \quad (10)$$

They propose instead that the ratio is buffered by some as yet unknown reaction. Polymerization reactions during melting of olivine and pyroxene provide a continuous supply of O^{2-} to the melt hence it is effectively buffered during mantle melting, and one must ask if free oxygen affects or controls Fe^{3+}/Fe^{2+} in MORBs.

The relationship between alkali content and elevated $Fe^{3+/}Fe^{2+}$ values of basaltic rocks is well established (e.g., Kress and Carmichael, 1989; 1988; Fudali, 1965; Paul and Douglas, 1965 and references therein) and was referred to as the *alkali-ferric iron effect* by Carmichael and Nicholls (1967). The O 1s XPS studies of Nesbitt et al. (2011) and Sawyer et al. (2015; 2012) demonstrate that the O^{2-} content of binary Na_2O-SiO_2 and K_2O-SiO_2 glasses (and melts) increases with alkali content. The same relationship is expected in basaltic magmas where elevated levels of alkali oxides should result in elevated O^{2-} contents. Elevated free oxygen values should force Reaction 9 to the right increasing the Fe^{3+}/Fe^{2+} values of alkali basalts over those of tholeiitic basalts. The experimental results of Borisov et al. (2017) and Cicconi et al. (2015) confirm that enhanced Na_2O, K_2O or CaO in basaltic-andesitic melts increases $Fe^{3+}/(Fe^{2+}+Fe^{3+})$ and we suggest that the increased ferric content results from enhanced O^{2-}.

Crust and upper mantle

As previously discussed, basaltic-komatiitic glasses are appreciably more polymerized than their lherzolitic upper mantle source. The O^{2-} produced should in turn, drive Reaction 9 to the right from which it follows that basaltic and komatiitic melts are more oxidized than their upper mantle sources or their residues. This presupposes that the O^{2-} is strongly partitioned into the melt. Continual migration of melt to the crust should result in progressive increase in the size of the 'oxidized' crustal reservoir, making polymerization during partial melting of the mantle an important reaction in transfer free oxygen from the upper mantle to the crust.

Once emplaced in or on the crust, magmas cool with olivine, pyroxene and other minerals crystallizing. These minerals incorporate Fe^{2+} preferentially, forcing Reaction 9 to the left. Some of the oxygen species may be released ultimately to the atmosphere (e.g., O_2) and hydrosphere (e.g., O^{2-} to form OH^- and H_2O). Pursuit of these avenues may provide additional insight into the evolution of the redox state of the crust, upper mantle, and perhaps the hydrosphere and atmosphere. If, for example, early during the Earth's evolution a magma ocean existed, melting likely was accompanied by polymerization reactions and by production of O^{2-}. This strong base certainly would have modified the redox state of the melts, residues of melting, and subsequent crystallization products, perhaps affecting the composition of the atmosphere, hydrosphere, core, mantle and crust.

ACKNOWLEDGEMENTS

The authors thank Tony Withers for insightful discussion and for reading the manuscript. We also thank B. Mysen and another anonymous reviewer for reading the manuscript and offering numerous comments which resulted in a substantially improved manuscript. The authors thank their respective Universities and departments for logistical support during the

conduct of this research.

References

Bancroft, G.M., Nesbitt, H.W., Henderson, G.S., O'Shaughnessy, C., Withers, A.C., and Neuville, D.R. (2018) Lorentzian dominated lineshapes and linewidths for Raman symmetric stretch peaks (800-1200 cm^{-1}) in Q species of alkali silicate glasses/melts. Journal of Non-Crystalline Solids, 484, 72-83.

Bento, A.P., and Bickelhaupt, F.M. (2007) Nucleophilic Substitution at Silicon (SN2@Si) via a Central Reaction Barrier. Journal of Organic Chemistry, 72, 2201-2207.

Borisov, A., Behrens, H., and Holtz, F. (2017) Effects of strong network modifiers on Fe^{3+}/Fe^{2+} in silicate melts: an experimental study. Contributions to Mineralogy and Petrology, 172, 34 1-14.

Bouhfid, M.A., Gruener, G., Mysen, B.O., and Richet, P. (2002) Premelting and calcium mobility in gehlenite ($Ca_2Al_2SiO_7$) and pseudowollastonite ($CaSiO_3$). Physics and Chemistry of Minerals, 29, 655-662.

Bowen, N.L., and Andersen, O. (1914) The binary system MgO-SiO_2. American Journal of Science, 37, 487-500.

Brawer, S.A., and White, W.B. (1975) Raman spectroscopic investigation of the structure of silicate glasses. I. The binary alkali silicates. Journal of Chemical Physics, 53, 2421-2432.

Budd S. M. (1961) The mechanisms of chemical reaction between silicate glass and attacking agents. Physics and Chemistry of Glasses, 2, 111–114.

Carmichael, I.S.E., and Nicholls, J. (1967) Iron-Titanium Oxides and Oxygen Fugacities in Volcanic Rocks. Journal of Geophysical Research, 72, 4665-4687.

547 Cicconi, M.R., Giuli, G., Ertel-Ingrisch, W., Paris, E., and Dingwell, D.B. (2015) The effect of
548 the [Na/(Na+K)] ratio on Fe speciation in phonolitic glasses. American Mineralogist, 100,
549 1610-1619.

550 Cooney, T.F., and Sharma, S.K. (1990) Structure of glasses in the systems Mg_2SiO_4-Fe_2SiO_4,
551 Mn_2SiO_4-Fe_2SiO_4, Mg_2SiO_4-$CaMgSiO_4$, and Mn_2SiO_4-$CaMnSiO_4$. Journal of Non-
552 Crystalline Solids, 122, 10-32.

553 Cormack, A.N., Du, J., and Zeitler, T.R. (2002) Alkali ion migration mechanisms in silicate
554 glasses probed by molecular dynamics simulations. Physical Chemistry and Chemical
555 Physics, 4, 3193-3197.

556 Dalby, K.N., Nesbitt, H.W., Zakaznova-Herzog, V.P., and King, P.L. (2007) Resolution of
557 bridging oxygen signals from O 1s spectra of silicate glasses using XPS: Implications for
558 O and Si speciation. Geochimica et Cosmochimica Acta, 71, 4297–4313.

559 Davis, M.C., Sanders, K.J., Grandinetti, P.J., Gaudio, S.J., and Sabyasachi, S. (2011) Structural
560 investigations of magnesium silicate glasses by ^{29}Si 2D magic-angle flipping NMR.
561 Journal of Non-Crystalline Solids, 357, 2787–2795.

562 Davis, J.C. (1965) Advanced Physical Chemistry: Molecules, Structure and Spectra. The Ronald
563 Press Co., New York, 632 p.

564 Demiralp, E., Cagin, T., and Goddard, W.A. (1999) Morse Stretch Potential Charge Equilibrium
565 Force Field for Ceramics: Application to the Quartz-Stishovite Phase Transition and to
566 Silica Glass. Physical Review Letters, 82, 1708-1711.

567 Dimanov, A., and Ingrin, J. (1995) Premelting and High-Temperature Diffusion of Ca in
568 Synthetic Diopside: An Increase of the Cation Mobility. Physics and Chemistry of

569 Minerals, 22, 437-442.

570 Dimanov, A., and Jaoul, O. (1998) Calcium self-diffusion in diopside at high temperature:
571 implications for transport properties. Physics and Chemistry of Minerals, 26, 116-127.

572 Frantz, J.D., and Mysen, B.O. (1995) Raman spectra and structure of $BaO-SiO_2$, $SrO-SiO_2$ and
573 $CaO-SiO_2$ melts at 1600°C. Chemical Geology, 121, 155–176.

574 Frost, D.J. (2008) The upper mantle and transition zone. Elements, 4, 171-176.

575 Frost, D.J., and McCammon, C.A. (2008) The Redox State of Earth's Mantle, Annual Reviews
576 in Earth and Planetary Sciences, 36, 389-420.

577 Fudali, R.F. (1965) Oxygen fugacities of basaltic and andesitic magmas. Geochimica et
578 Cosmochimica Acta, 29, 1063–1075.

579 George, A.M., Richet, P., and Stebbins, J.F. (1998) Cation dynamics and premelting in lithium
580 metasilicate (Li_2SiO_3) and sodium metasilicate (Na_2SiO_3): A high-temperature NMR
581 study. American Mineralogist, 83, 1277-1284.

582 Goldman, D.S. (1983) Oxidation equilibrium of iron in borosilicate glass. Journal of the
583 American Ceramics Society, 66, 205-209.

584 Hamlin, T.A., Swart, M., and Bickelhaupt F.M. (2018) Nucleophilic Substitution (SN2):
585 Dependence on Nucleophile, Leaving Group, Central Atom, Substituents, and Solvent.
586 Chemical Physics Physical Chemistry, **19**, 1315-1330.

587 Holmquist, S.B. (1966) Ionic formulation of redox equilibria in glass melts. Journal of the
588 American Ceramics Society. 49, 228-229.

589 House, J.E. (1997) Principles of Chemical Kinetics. Wm. C. Brown Publishers, Dubuque IA.,
590 244 p.

591 Hsieh, C.H., Jain, H., Miller, A.C., and Kamitsos, E.I. (1994) X-ray photoelectron spectroscopy
592 of A1- and B-substituted sodium trisilicate glasses. Journal of Non-Crystalline Solids, 168,
593 247-257.
594 Johnston, W.D. (1965) Oxidation-reduction equilibria in $Na_2O•2SiO_2$ glass. Journal of the
595 American Ceramics Society, 48, 184-190.
596 Kalampounias, A.G., Nasikas, N.K., and Papatheodorou, G.N. (2009) Glass formation and
597 structure in the $MgSiO_3$–Mg_2SiO_4 pseudobinary system: From degraded networks to ionic-
598 like glasses. Journal of Chemical Physics, 131, 114513 – 1-114513 – 8.
599 Kohara, S., Akola, J., Morita, H., Suzuya, K., Weber, J.K.R., Wilding, M.C., and Benmore, C.J.
600 (2011) Relationship between topological order and glass forming ability in densely packed
601 enstatite and forsterite composition glasses. Proceedings of the National Academy of
602 Sciences, 108, 14780-14785.
603 Kohara, S., Suzuya, K., Takeuchi, K., Loong, C.-K., Grimisditch, M., Weber, J.K.R., Tangeman,
604 J.A., and Key, T.S. (2004) Glass formation at the limit of insufficient network formation.
605 Science, 303, 1649-1652.
606 Kracek, F.C., Bowen, N.L., and Morey, G.W. (1937) Equilibrium relations and factors
607 influencing their determination in the system K_2SiO_3-SiO_2. Journal of Physical Chemistry,
608 41, p. 1183-1193.
609 Krauskopf, K.B., and Bird, D.K. (1995) Introduction to Geochemistry. (3rd edition), McGraw-
610 Hill Inc. New York, 647 p.
611 Kress, V.C., and Carmichael, I.S.E. (1988) Stoichiometry of the iron oxidation reaction in
612 silicate melts. American Mineralogist, 73, 1267-1274.

613 Kress, V.C., and Carmichael, I.S.E. (1989) The lime-iron-silicate melt system: Redox and
614 volume systematics. Geochimica et Cosmochimica Acta, 33, 2883-2892.
615 Laidler, K.J. (1965) Chemical Kinetics. (2nd edition), McGraw-Hill Book Co., New York, 566 p.
616 Maekawa, H., Maekawa, T., Kawamura, K., and Yokokawa, T. (1991) The structural groups of
617 alkali silicate glasses determined from ^{29}Si MAS-NMR. Journal of Non-Crystalline Solids,
618 127, 53-64.
619 Magnien, V., Neuville, D.R., Cormier, L., Roux, J., Hazeman, J-L., de Ligny, D., Pascarelli, S.,
620 Vickridge, I., Pinet, O., and Richet, P. (2008) Kinetics and mechanisms of iron redox
621 reactions in silicate melts: The effects of temperature and alkali cations. Geochimica et
622 Cosmochimica Acta, 72, 2157-2168.
623 Masson, C.R., Smith, I.B., and Whiteway, S.G. (1970) Activities and ionic distributions in liquid
624 silicates: application of polymer theory. Canadian Journal of Chemistry, 48, 1456–1464.
625 McMillan, P.F., 1984. Structural studies of silicate glasses and melts-applications and limitations
626 of Raman spectroscopy. American Mineralogist, 69, 622-644.
627 Moellwyn-Hughes, E.A. (1961) Physical Chemistry. (2nd Edition), Pergamon Press, Oxford,
628 1334 pp.
629 Morizet, Y., Vuilleumier, R., and Paris, M. (2015) A NMR and molecular dynamics study of
630 CO_2-bearing basaltic melts and glasses. Chemical Geology, 418, 89-103.
631 Mysen, B.O., and Frantz, J.D. (1992) Raman spectroscopy of silicate melts at magmatic
632 temperatures: Na_2O-SiO_2, K_2O-SiO_2 and Li_2O-SiO_2 binary compositions in the
633 temperature range 25-1475°C. Chemical Geology, 96, 321-332.
634 Mysen, B.O., and Frantz, J.D. (1993) Structure and properties of alkali silicate melts at

magmatic temperatures. European Journal of Mineralogy, 5, 393-407.

Mysen, B.O., and Frantz, J.D. (1994) Silicate melts at magmatic temperatures: in-situ structure determination to 1651ºC and effect of temperature and bulk composition on the mixing behavior of structural units. Contributions to Mineralogy and Petrology, 117, 1-14.

Mysen, B.O., and Richet, P. (2019) Silicate glasses and melts, (2^{nd} edition), Elsevier Science, 728 pp.

Nasikas, N.K., Chrissanthopoulos, A., Bouropoulos, N., Sen, S., and Papatheodorou, G.N. (2011). Silicate glasses at the ionic limit: Alkaline-earth sub-orthosilicates. Chemistry of Materials, 23, 3692–3697.

Nasikas, N.K., Edwards, T.G., Sen, S., and Papatheodorou, G.N. (2012) Structural Characteristics of novel Ca-Mg orthosilicate and suborthosilicate glasses: Results from ^{29}Si and ^{17}O NMR spectroscopy. Journal of Physical Chemistry B, 116, 2696–2702.

Naylor, B.F. (1945) High-temperature heat contents of sodium metasilicate and sodium disilicate. Journal of the American Chemical Society, 67, 466-467.

Nesbitt, H.W., Bancroft, G.M., Henderson, G.S., Ho, R., Dalby, K.N., Huang, Y., and Yan, Z. (2011) Bridging, non-bridging and free (O^{2-}) oxygen in Na_2O-SiO_2 glasses: An X-ray Photoelectron Spectroscopic (XPS) and Nuclear Magnetic Resonance (NMR) study. Journal of Non-Crystalline Solids, 357, 170-180.

Nesbitt, H.W., Bancroft, G.M., Henderson, G.S., Sawyer, R., and Secco, R.A. (2015) Direct and Indirect Evidence for Free Oxygen (O^{2-}) in MO-Silicate Glasses and Melts (M = Mg, Ca, Pb). American Mineralogist, 100, 2566-2578.

Nesbitt, H.W., Bancroft, G.M., Henderson, G.S., Richet, P., and O'Shaughnessy, C. (2017a)

Melting, crystallization and the glass transition: toward a unified description for silicate phase transitions. American Mineralogist, 102, 412-420.

Nesbitt, H.W., Cormack, A.N. and Henderson, G.S. (2017b) Defect contributions to the heat capacities and stabilities of some chain, ring, and sheet silicates, with implications for mantle minerals. American Mineralogist, 102, 2220-2229.

Nesbitt, H.W., Henderson, G.S., Bancroft, G.M., Sawyer, R., and Secco, R.A. (2017c) Bridging oxygen speciation and free oxygen (O^{2-}) in K-silicate glasses: Implications for spectroscopic studies and glass structure. Journal of Non-Crystalline Solids, 461, 13-22.

Nesbitt, H.W., Bancroft, G.M., and Ho., R. (2017d) XPS valence band study of Na-silicate glasses: energetics and reactivity. Surface and Intefacial Analysis, 49, 1298-1308.

Orr, R.L. (1953) High Temperature Heat Contents of Magnesium Orthosilicate and Ferrous Orthosilicate. Journal of the American Chemical Society, 75, 528-529.

Paul, A., and Douglas, R.W. (1965) Ferrous-ferric equilibrium in binary alkali silicate glasses. Physics and Chemistry of Glasses, 6, 207-11.

Piriou, B., and McMillan, P. (1983) The high-frequency vibrational spectra of vitreous and crystalline orthosilicates. American Mineralogist, 68, 426-443.

Retsinas, A., Kalampounias, A.G., and Papatheodorou, G.N. (2014) Reaching the ionic limit in the $(1-X)[Ca_{0.5}\text{-}Mg_{0.5}]O–X_{SiO2}$ pseudo binary glass system with $0.5 < X < 0.27$: Glass formation and structure. Journal of Non-Crystalline Solids, 383, 38–43.

Richet P. (2001) Glasses and the Glass Transition. Chap. 15, in Solid Solutions in Silicate and Oxide Systems (ed. C.A. Geiger). EMU Notes in Mineralogy, European Mineralogical Union, Eötvös University Press, Budapest, p. 419-447.

679 Richet, P., and Bottinga, Y. (1986) Thermochemical Properties of Silicate Glasses and Liquids'
680 A Review. Reviews in Geophysics, 24, 1-25.
681 Richet, P., Bottinga, Y., and Téqui, C. (1984) Heat capacity of sodium silicate liquids. Journal of
682 the American Ceramics Society. 67, C6-C8.
683 Richet, P., Bottinga, Y., Denielou, L., Petitet, J.P., and Téqui, C. (1982) Thermodynamic
684 properties of quartz, cristobalite and amorphous SiO_2: drop calorimetry measurements
685 between 1000 and 1800 K and a review from 0 to 2000 K. Geochimica et Cosmochimica
686 Acta, 46, 2639-2658.
687 Richet, P., and Fiquet, G. (1991) High-temperature heat capacity and premelting of minerals in
688 the system MgO-CaO-Al_2O_3-SiO_2. Journal of Geophysical Research, 96, 445-456.
689 Richet, P., Ingrin, J., Mysen, B.O., Courtial, P., and Gillet, P. (1994) Premelting effects in
690 minerals: an experimental study. Earth and Planetary Science Letters, 121, 589-600.
691 Richet, P., Leclerc, F., and Benoist, L. (1993) Melting of forsterite and spinel, with implications
692 for the glass transition of Mg_2SiO_4 liquid. Geophysical Research Letters, 20, 1675-1678.
693 Richet, P., Mysen, B.O., and Andrault, D. (1996) Melting and premelting of silicates: Raman
694 spectroscopy and X-ray diffraction of Li_2SiO_3 and Na_2SiO_3. Physics and Chemistry of
695 Minerals. 23, 157-172.
696 Richet, P., Mysen, B.O., and Ingrin, J. (1998) High-temperature X-ray diffraction and Raman
697 spectroscopy of diopside and pseudowollastonite. Physics and Chemistry of Minerals, 25,
698 401-414.
699 Sawyer, R., Nesbitt, H.W., Bancroft, G.M., Thibault, Y., and Secco, R.A. (2015) Spectroscopic
700 studies of oxygen speciation in potassium silicate glasses and melts. Canadian Journal of

Chemistry, 93, 60–73.

Sawyer, R., Nesbitt, H.W., and Secco, R.A. (2012) Three types of oxygen in K_2O-SiO_2 glasses, an X-ray photoelectron spectroscopy (XPS) study. Journal of Non-Crystalline Solids, 358, 290-302.

Schneider, J., Mastelaro, V.R., Panepucci, H., and Zanotto, E.D. (2000) ^{29}Si MAS-NMR studies of Q^n structural units in metasilicate glasses and their nucleating ability. Journal of Non-Crystalline Solids, 273, 8-18.

Sen, S., and Tangeman, J. (2008) Evidence for anomalously large degree of polymerization in Mg_2SiO_4 glass and melt. American Mineralogist, 93, 946-949.

Sen, S., Maekawa, H., and Papatheodorou, G.N. (2009) Short-range structure of invert glasses along the pseudo-binary join $MgSiO_3$-Mg_2SiO_4: results from ^{29}Si and ^{25}Mg NMR spectroscopy. Journal of Physical Chemistry, 113, 15243-15248.

Sharma, S.K., Yoder, H.S., and Matson, D. W. (1988) Raman study of some melilites in crystalline and glassy states. Geochimica et Cosmochimica Acta, 52, 1961-1967.

Speight, J.G. (2005) Lange's Handbook of Chemistry 70th Anniversary Edition. McGraw Hill Standard Handbook, New York, Table 4.11, p. 4.41-4.51.

Stebbins, J.F. (1987). Identification of multiple structural species in silicate glasses by ^{29}Si NMR. Nature, 330, 465–467.

Swamy, V., and Dubrovinsky, L.S. (1997) Thermodynamic data for the phases in the $CaSiO_3$ system. Geochimica et Cosmochimica Acta, 61, 1181-1191.

Thiéblot, L., Téqui, C., and Richet, P. (1999) High-temperature heat capacity of grossular ($Ca_3Al_2Si_3O_{12}$), enstatite ($MgSiO_3$), and titanite ($CaTiSiO_5$). American Mineralogist, 84,

848-855.

Toop, G.W., and Samis, C.S. (1962a) Activities of ions in silicate melts. Transactions of the Metallurgical Society of America Institute in Mining Engineering, 224, 878–887.

Toop, G.W., and Samis, C.S. (1962b) Some new ionic concepts of silicate slags. Canadian Metallurgical Quarterly, 1, 129–152.

Voronko, Yu. K., Sobol, A.A., and Shukshin, V.E. (2006) Raman Spectra and Structure of Silicon–Oxygen Groups in Crystalline, Liquid, and Glassy Mg_2SiO_4. Inorganic Materials, 42, 981-988.

Zhang, P., Grandinetti, P.J., and Stebbins, J.F. (1997) Anionic Species Determination in $CaSiO_3$ Glass Using Two-Dimensional ^{29}Si NMR. Journal of Physical Chemistry, 101, 4004-4008.

Figure Captions

Fig. 1: ^{29}Si MAS NMR and Raman spectra of Mg_2SiO_4 glass. (a) ^{29}Si NMR spectrum of Mg_2SiO_4 collected at ambient temperature where the dotted curve represents the spectrum. Peak assignments and intensities are from Sen and Tangeman (2008). The solid curve represents our estimate of the Q^2 band intensity (~10% of total glass spectrum). (b) Raman spectrum of Mg_2SiO_4 glass. The fitted peak is 50% Lorentzian, 50% Gaussian with a Raman shift of 870 cm^{-1} and FWHM of 60 cm^{-1}. It is interpreted as a Q^0 peak and represents ~50% of the area under the spectrum.

Fig. 2: (a) Illustrates the Raman spectrum of crystalline Na_2SiO_3 collected 14 K below its melting temperature. The thick solid curve is redrawn after Richet et al. (1996). The fit and peak assignments are those of Nesbitt et al. (2017a). (b) Illustrates the Raman spectrum of liquid Na_2SiO_3 collected 1 K above its melting temperature. The thick solid curve and the fit are redrawn after Richet et al. (1996). Peak assignments are ours and peak areas have been estimated from the fit of Richet et al. (1996).

Fig. 3: Reaction mechanisms associated with formation of Q^1 and Q^2 species in Mg_2SiO_4 melt/glass. All reactions shown are nucleophilic in nature. (a) Illustrates the attack of NBO^- (a nucleophile) on a Si center of a Q^0 species to form a pentahedrally coordinated Si activated complex which decays to produce a Si_2O_7 moiety (two Q^1 species) and O^{2-}. (b) Illustrates the attack of the nucleophile NBO^- on Si of a Q^1 species to form an intermediate reaction product, Si^V (an activated complex), which produces a Si_3O_{10} moiety containing a Q^2 species and two Q^1 species and O^{2-}.

Fig. 4: Nucleophilic reaction mechanisms affecting Q^2 chains. (a) Reaction whereby an infinite

Q^2 chain is fragmented with Q^1 species produced as termini to each Q^2 fragment. (b) Reaction whereby a Q^1 species is reacted with a Q^2 species of an adjacent chain to produce a Q^3 species and O^{2-}.

Fig. 5: Illustrates librational and rotational modes available to Q^1 species where all NBO^- are 'unpinned' (i.e., not restricted to its structural position after NBO-M bond rupture), as explained in the text. With dissociation of the three NBO-M bonds, the molar contribution of Q^1 to the C_p of the melt almost doubles. 'Unpinned' NBO^- of Q^0 species may undergo full rotation with sufficient thermal agitation. (b) C_p of Na_2SiO_3 crystal and melt are illustrated by the shaded circles (Nesbitt et al., 2017b; Richet et al., 1996; 1984; Naylor, 1945). The premelting region of the crystal is shaded emphasizing the dramatic increase in C_p as the melting point is approached. The dashed curve represents the Debye vibrational contribution to the C_p of Na_2SiO_3 and the solid curve represents the Debye contribution *plus* the contributions due to bond dissociation and defect formation (Nesbitt et al., 2017b). These contributions alone do not explain the increased C_p of the premelting region.

Fig. 6: (a) Hypothetical chains of Q^2 species where NBO-M bonds are ruptured on a Q^2 species allowing it to undergo ***limited*** libration about its BO-BO axis, as in 'i'. With sufficient thermal agitation, the librating Q^2 species may top its local potential energy well to undergo ***pronounced*** libration, as in 'ii'. With still greater thermal agitation, the Q^2 species may undergo full rotation about it BO-BO axis by topping the maximum in the potential energy curve, as in 'iii'. (b) Hypothetical potential energy curve associated with hindered and full rotation of a Q^2 species about its BO-BO axis of a chain of Q^2 species.

This is a preprint, the final version is subject to change, of the American Mineralogist (MSA)
Cite as Authors (Year) Title. American Mineralogist, in press.
DOI: https://doi.org/10.2138/am-2020-6841

778

Table 1: Q Speciation in Binary Silicate Glasses

Glass/Melt Composition	Q^0 %	Q^1 %	Q^2 %	Q^3 %	Q^4 %	O^{2-} %[2]	NBO/Si[1]	Reference
Mg_2SiO_4	44	46	10			8.3	3.34	Sen and Tangeman (2008)
Mg_2SiO_4	63	37				4.6	3.63	Davis et al. (2011)
Mg_2SiO_4	60	40				5.0	3.60	Sen et al. (2009)
Mg_2SiO_4	~50	__ ~50__[3]				>6		Voronko et al. (2006)
Mg_2SiO_4	49	31	14	6		9.6	3.23	Kalampounias et al. (2009)
$CaMgSiO_4$	50	35	13	2		8.4	3.33	Nasikas et al. (2011)
$CaMgSiO_4$	61	39				4.9	3.61	Nasikas et al. (2012)
Fe_2SiO_4	<50	__ >50 __[4]				>10		Cooney and Sharma (1990)
$MgSiO_3$	0	25	42	25.7	7.3	2.6	1.85	Sen et al. (2009)
$MgSiO_3$	1.4	19.1	53.0	25.2	1.4	1.0	1.94	Davis et al. (2011)
$CaSiO_3$	0.7	19.3	54.7	24.2	1.1	0.9	1.94	Zhang et al. (1997)
$CaMgSi_2O_6$	4.6	7.5	34.0	53.8	0	6.2	1.63	Retsinas et al. (2014)
$CaMgSi_2O_6$	0	28	43	25	4	0.8	1.95	Schneider et al. (2000)

1 NBO/Si = $(4Q^0+3Q^1+2Q^2+1Q^3)/(Q^0+Q^1+Q^2+Q^3+Q^4)$

2 mol% O^{2-} = 100x[(NBO/T)stoichiometric - NBO/T)observed]/(2xTotal Oxygen) where (NBO/T)stoichiometric = 4.0 for the orthosilicate glasses and 2.0 for metasilicates. (NBO/T)stoichiometric should be calculated from the reported glass composition. Total oxygen = 4.0 for orthosilicates and 3.0 for metasilicates glasses and melts.

3 sum of Q^1 and Q^2 species is ~50%

4 sum of Q^1 and Q^2 species is greater than 50%

779

This is a preprint, the final version is subject to change, of the American Mineralogist (MSA)
Cite as Authors (Year) Title. American Mineralogist, in press.
DOI: https://doi.org/10.2138/am-2020-6841

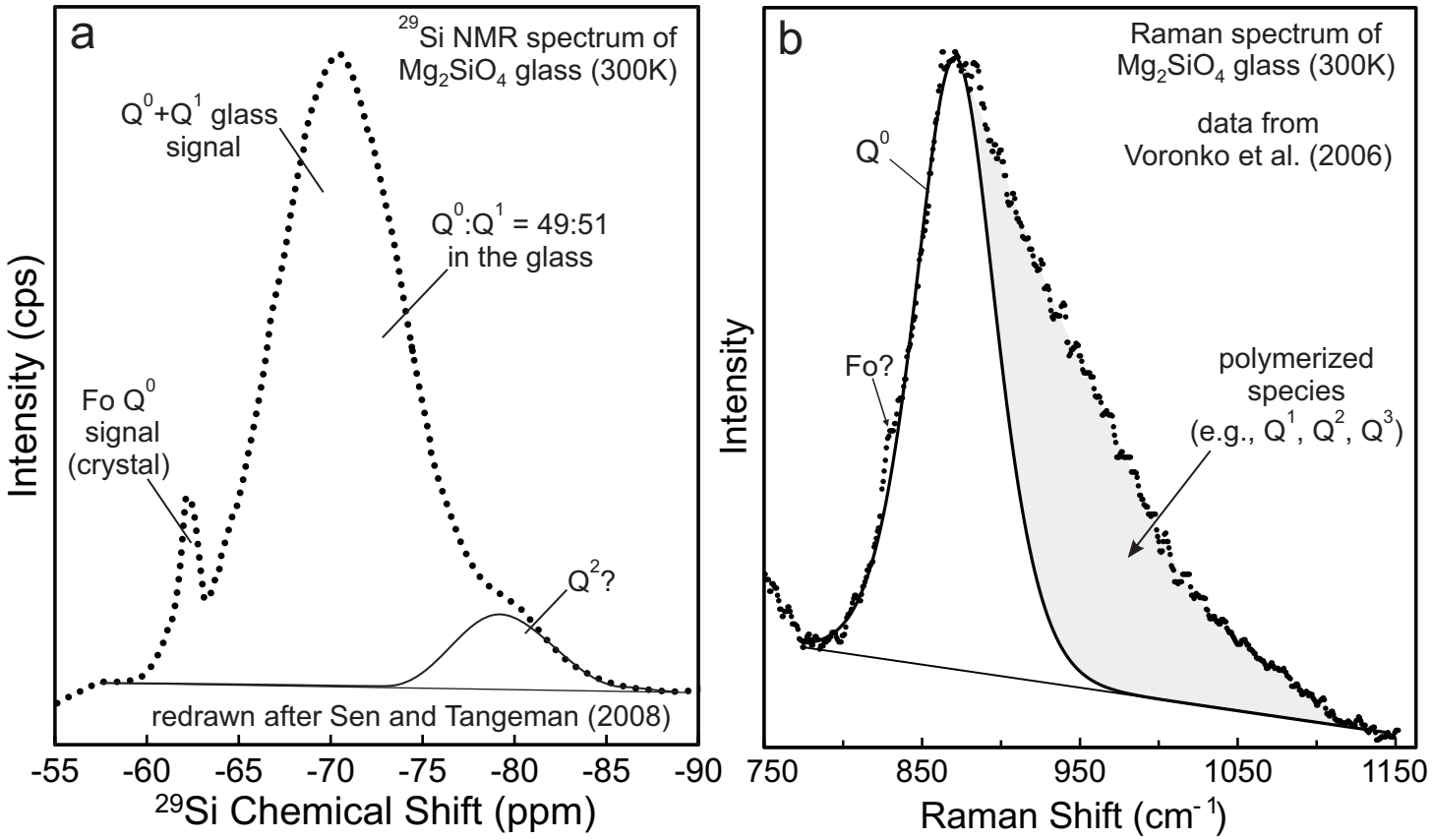

Fig. 1

This is a preprint, the final version is subject to change, of the American Mineralogist (MSA)
Cite as Authors (Year) Title. American Mineralogist, in press.
DOI: https://doi.org/10.2138/am-2020-6841

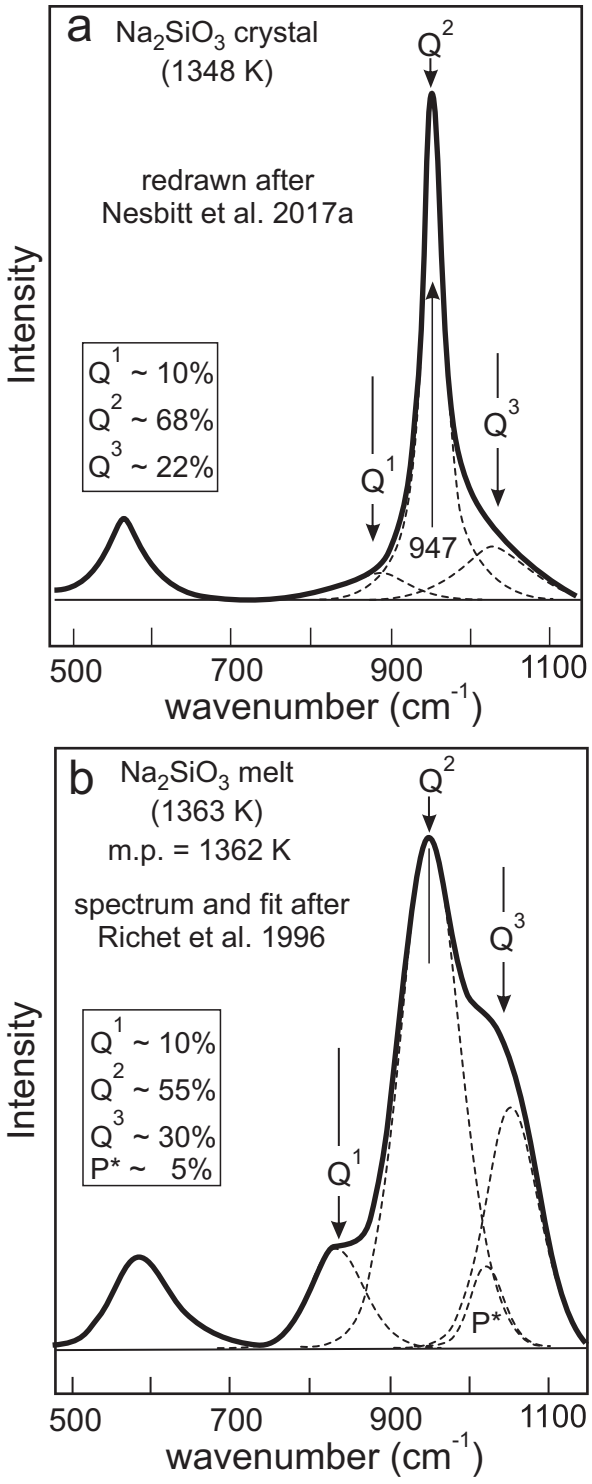

Fig. 2

This is a preprint, the final version is subject to change, of the American Mineralogist (MSA)
Cite as Authors (Year) Title. American Mineralogist, in press.
DOI: https://doi.org/10.2138/am-2020-6841

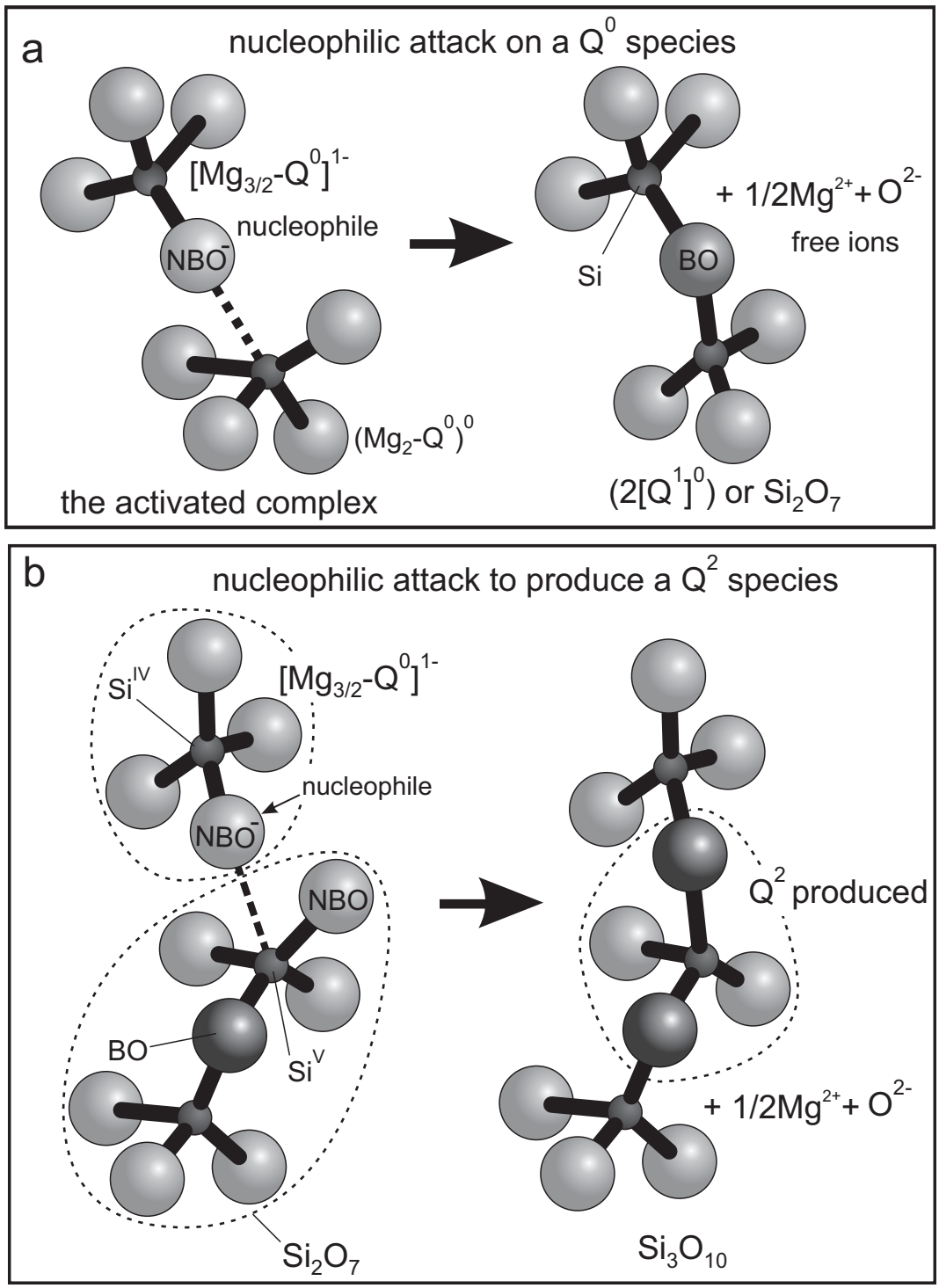

Fig. 3

This is a preprint, the final version is subject to change, of the American Mineralogist (MSA)
Cite as Authors (Year) Title. American Mineralogist, in press.
DOI: https://doi.org/10.2138/am-2020-6841

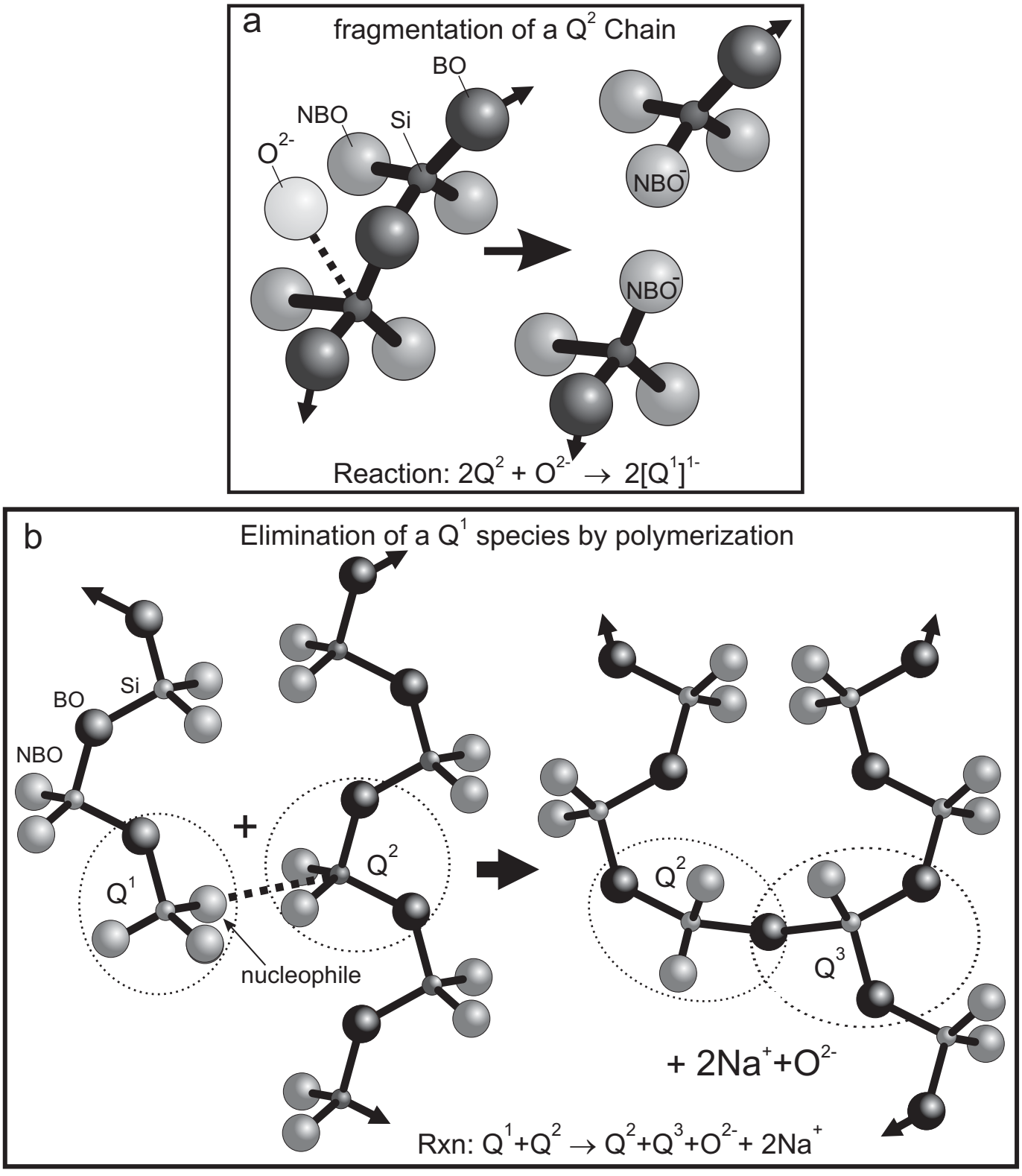

Fig. 4

This is a preprint, the final version is subject to change, of the American Mineralogist (MSA)
Cite as Authors (Year) Title. American Mineralogist, in press.
DOI: https://doi.org/10.2138/am-2020-6841

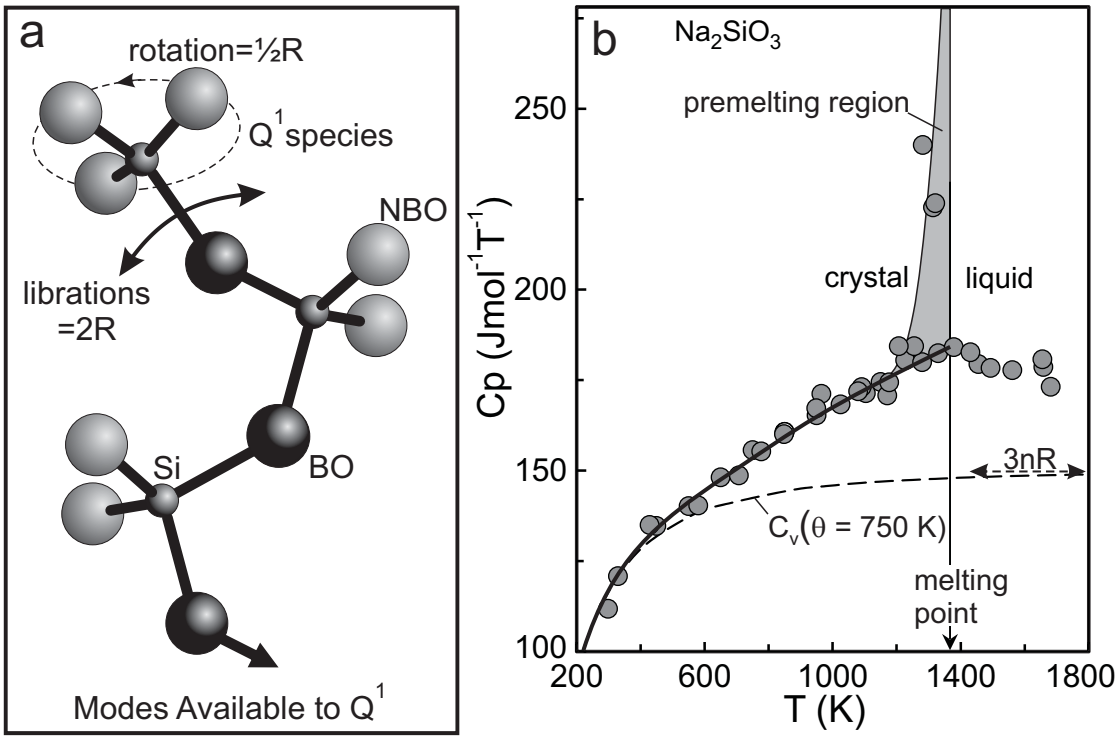

Fig. 5

This is a preprint, the final version is subject to change, of the American Mineralogist (MSA)
Cite as Authors (Year) Title. American Mineralogist, in press.
DOI: https://doi.org/10.2138/am-2020-6841

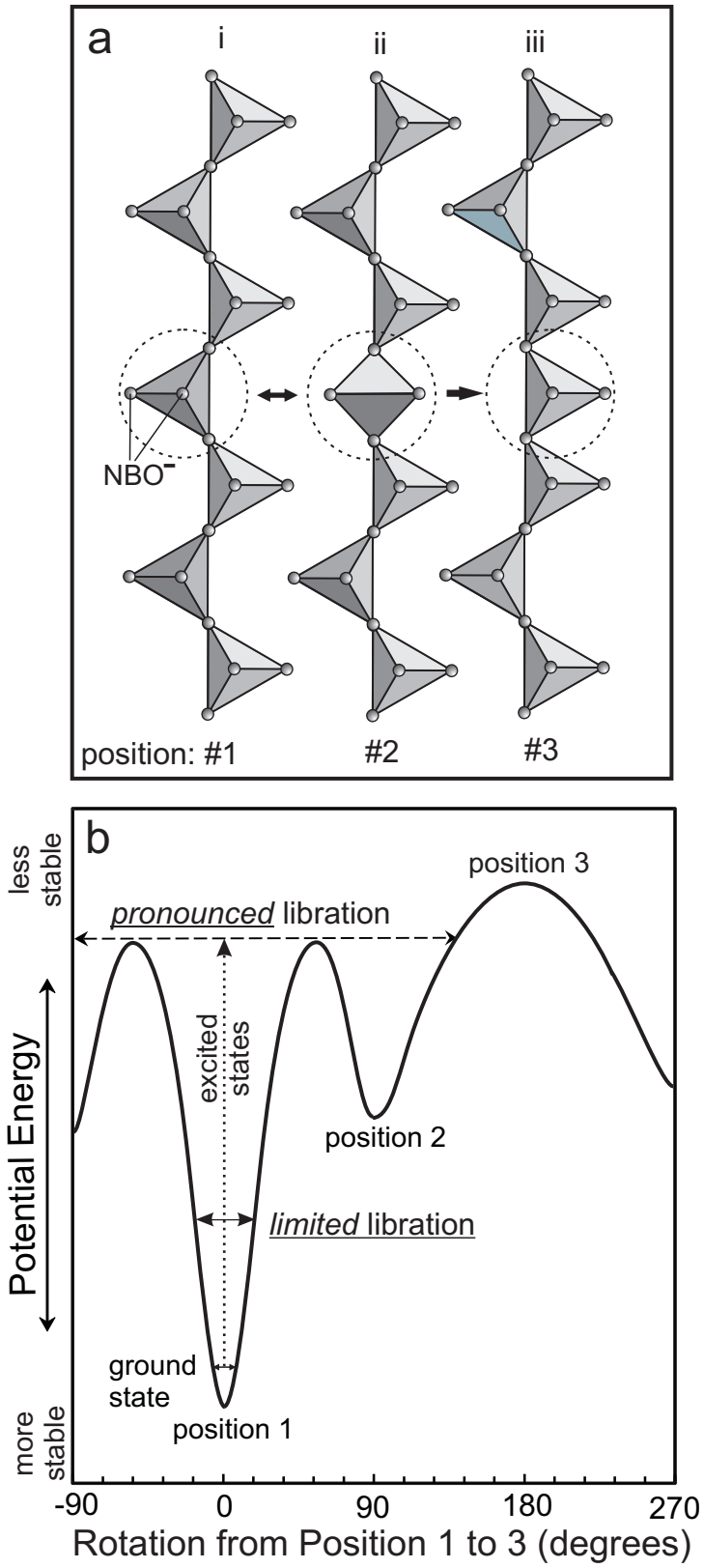

Fig. 6